# High-strength and high-conductivity casting Al-1.8Fe-Mg-Si alloy obtained by regulating the Mg/Si ratio

Yu-fei Zhang<sup>1,+</sup>, Xi-long Luo<sup>1,+</sup>, Zheng-hao Shao<sup>1</sup>, Qun Luo<sup>1,\*</sup>, Bin Hu<sup>2</sup>, Hong-zhou Lu<sup>3</sup>, and Qian Li<sup>1,2,4,\*</sup>

- 1. School of Materials Science and Engineering, Shanghai University, Shanghai, 200444, China
- 2. Chongqing Institute of New Energy Storage Materials and Equipment, Chongqing, 401135, China

3. CITIC Metal Co. Ltd, Beijing, 100004, China

4. College of Materials Science and Engineering, National Engineering Research Center for Magnesium Alloys, National Key Laboratory of Advanced Casting Technologies, Chongqing University, Chongqing, 400044, China \*Corresponding address: e-mail: qunluo@shu.edu.cn (Qun Luo), cquliqian@cqu.edu.cn (Qian Li)

Abstract: The Al-1.8Fe eutectic alloy is considered a potential substitute for Cu conductors due to its low resistivity and excellent casting performance. In this work, the second phase in Al-1.8Fe is modified by adding Mg and Si, and at the same time, the heat treatment properties of the alloy are changed. The combined addition of Mg and Si significantly refines the second phase of the Al-1.8Fe alloy and increases the second phase fraction. The tensile strength of as-cast Al-1.8Fe-0.45Mg-0.5Si alloy reaches 184.8 ± 2.4 MPa. But the solid solution of Mg and Si causes significant lattice distortion, and the electrical conductivity is reduced to 45.6 ± 0.4 %IACS. The T6 heat treatment realizes the synergistic improvement of the mechanical properties and electrical conductivity of the Al-1.8Fe alloy, but the content of Mg and Si shows a non-positive correlation with the properties of the alloy after heat treatment. When the Mg/Si ratio is between 0.9 and 1.2, the Al-1.8Fe-Mg-Si alloy shows the best aging strengthening effect. The tensile strength of peak-aged Al-1.8Fe-0.45Mg-0.5Si alloy reaches 309.5 MPa, and the electrical conductivity reaches 52.5 %IACS. This work offers a solution idea to the mismatch between mechanical properties and electrical conductivity in casting aluminum alloys.

Keywords: Al-Fe alloys; Second phases; T6 heat treatment; electrical conductivity; mechanical properties;

### 1 Introduction

In recent years, with the advancement of the country's "dual-carbon" goal and the implementation of energy conservation and emission reduction policies, new energy vehicles, due to their low energy consumption (11.9 kWh/100 km), are gradually becoming the main alternative to fuel vehicles (45 kWh/100 km)[1, 2]. As a core component, the performance of the motor directly affects the power output and energy efficiency of the vehicle<sup>[3]</sup>. With the advancement of drive technology, the rotational speed of the motor rotor is constantly increasing, and the maximum speed can reach 20,000 rpm. This puts forward higher requirements for the mechanical strength, electrical conductivity, and heat resistance of the rotor material. Aluminum alloy, with its high specific strength, low cost, and excellent electrical and thermal conductivity, has become the primary choice for rotor materials<sup>[4-6]</sup>. However, existing commercial aluminum alloy systems have difficulty meeting the requirements of high conductivity and high strength simultaneously. For example, the strength of commercial A356 alloy<sup>[7-10]</sup> is approximately 250 MPa, but its electrical conductivity is less than 40 %IACS. The electrical conductivity of commercial 1070 alloy<sup>[11]</sup> is as high as 60 %IACS, but its strength is less than 30 MPa. The rotor material of the drive motor for new energy vehicles needs to maintain an electrical conductivity of not less than 50 %IACS and a yield strength of not less than 60 MPa at a service working temperature of 180 °C<sup>[12]</sup>. Therefore, the development of new aluminum alloys with both high electrical conductivity and high strength has become an urgent problem to be solved.

In the traditional strengthening mechanism, solid solution elements, second phases, grain boundaries, and dislocations are considered the main factors affecting the strength of alloys. However, since these factors have a scattering effect on electron propagation, it leads to an inherent mismatch between strength and electrical conductivity<sup>[13-15]</sup>. Due to its precipitation behavior and

age-hardening effect, the Al-Mg-Si alloy exhibits mechanical excellent properties and electrical conductivity after artificial aging treatment<sup>[15-17]</sup>. Dong et al.[18] influenced the type and size of precipitates by adjusting the Mg/Si ratio, and achieved a synergistic improvement of the strength and electrical conductivity of the Al-Mg-Si alloy during the aging process. However, with the progress of aging, these precipitates will transform and coarsen, resulting in a decrease in the strength of the aluminum alloy[19]. Therefore, the Al-Mg-Si alloy shows instability in mechanical properties in a high-temperature environment.

The alloying elements dissolved in the aluminum matrix are the decisive factors affecting the electrical conductivity. Since the solid solubility of Fe element in the aluminum matrix at room temperature is only 0.052 wt.%, its impact on the electrical conductivity is much lower than that of the second phase<sup>[20, 21]</sup>. Therefore, Al -Fe alloys have been applied to motor rotors and electrical transmission devices<sup>[22-26]</sup>. However, as a new type of cast aluminum alloy, the coarse Fe- rich phase in as-cast Al-Fe alloys reduced the formability and workability of the alloy. Researchers usually adopt micro-alloying to improve this problem. Luo et al. [27] refined the grains and optimized the morphology of the Al<sub>3</sub>Fe phase by adding Ce. Kong et al.[28] studied the effects of the combined addition of Zr and Er on the Al-0.4Fe alloy, transforming the acicular Al<sub>3</sub>Fe phase into fine rod-shaped particles and improving the strength and electrical conductivity. Shi et al.[29] proposed that Ce can also promote the formation of a discontinuous network or granular structure of the Fe-rich phase, improving the alloy's uniformity and mechanical properties. Shin et al.[30] found that the Fe-rich phase and solidification process in the Al-1Fe alloy are not affected by the initial Si/Fe ratio, but depend on the segregation of Si and the content of Mg. Trink et al.[31] proposed that by adding Mg and Si to the Al - Fe alloy, it can be given age-hardening ability, thereby improving its comprehensive properties. In addition, research shows that adding Ni can effectively refine the grains and improve the morphology of the Fe-rich phase, forming a finer Al<sub>9</sub>FeNi phase<sup>[32, 33]</sup>. This change often leads to better mechanical properties and electrical conductivity. The high-temperature stability of the Al-Fe-Ni alloy is caused by the Al<sub>9</sub>FeNi phase with a low coefficient of thermal expansion<sup>[34]</sup>. In addition, by changing the Fe/Ni ratio, the morphology of the second phase in the alloy can be affected and its microstructure can be adjusted<sup>[35]</sup>. Kim et al.<sup>[36]</sup> pointed out that for die-cast Al-0.5Fe alloy, with the increase of Ni content, the Al<sub>3</sub>Ni phase is preferentially formed in the alloy instead of the Al<sub>9</sub>FeNi phase. Pan and Breton<sup>[12]</sup> proposed the influence of Ni content on the Al-1.7Fe alloy. The addition of Ni promotes the formation of both coarse primary Al<sub>9</sub>FeNi phase and fine eutectic Al<sub>9</sub>FeNi phase.

At present, in the research on Al-Fe-based alloys, a corresponding relationship systematic among composition, microstructure, mechanical properties and electrical conductivity has not been established. This paper focuses on the Al-1.8Fe alloy, studies the influence mechanism of different Mg and Si contents and Mg/Si ratios on the types and morphologies of the second phase and their effects on the electrical conductivity and mechanical properties of the alloy, and also studies the evolution of the microstructure and properties of the Al-1.8Fe-xMg-ySi alloy during the heat treatment. Through micro-alloying and age-hardening, morphology and distribution of the second phase, element distribution and nano-precipitates are regulated, and a casting Al-1.8Fe-0.45Mg-0.5Si alloy with both high strength and high electrical conductivity is obtained.

### 2 Experimental

The Al-1.8Fe-xMg-ySi alloys listed in Table 1 were prepared using industrial pure aluminum, Al-20Fe master alloy, Al-50Mg master alloy and Al-20Si master alloy. These raw materials were placed in the clean graphite crucible and heated in the resistance furnace during the melting process. The aluminum granules were first melted at 800 °C. Pre-dried Fe granules and Ni powder were added, followed by one-hour insulation to ensure complete melting. Then, the melt was held at a lower temperature of 740 °C for 1 h. During the holding process, stirring is performed for 30 s every 30 min to ensure uniform composition of the melt. The obtained homogenous melt was purified using 0.5 wt.% Foseco refining agent. Pure Ar gas was introduced for 3 minutes for further degassing and impurity removal. Subsequently, the melt was poured into the  $\Phi$ 30 mm cylindrical steel mold and the permanent mold for  $\Phi 10$  mm tensile bar, respectively. And the molds are preheated at 250 °C.

This study used Inductively Coupled Plasma Atomic Emission Spectroscopy (ICP-AES) to determine the chemical compositions of the cast alloys, proving the rationality of the casting process.

The phase constitutions of these as-cast alloys were analyzed via X-ray diffraction (XRD, Bruker D8) with a scanning range of 20 to 50° at a speed of 2 °/min. The polished alloys were immersion corroded in the 5%

NaOH aqueous solution for 20-30 seconds, followed by observation of the microstructure and phase characteristics using scanning electron microscopy (SEM, Hitachi FLEX-1000). The phase compositions were analyzed using energy dispersive spectrometry (EDS).

Table 1. Nominal and actual compositions of Al-1.8Fe-Mg-Si alloy

The hardness test of the alloy was conducted using

Samples	Nominal composition (wt.%)	Actual composition (wt.%)	Mg/Si ratio
0Mg-0Si	Al-1.8Fe	Al-2.32Fe	/
0.45Mg-0Si	Al-1.8Fe -0.45Mg	Al-2.06Fe -0.74Mg	/
0.3Mg-0.5Si	Al-1.8Fe -0.3Mg-0.5Si	Al-2.28Fe -0.54Mg-0.38Si	0.6
0.45Mg-0.7Si	Al-1.8Fe -0.45Mg-0.7Si	Al-2.38Fe -0.61Mg-0.61Si	0.6
0.45Mg-0.5Si	Al-1.8Fe -0.45Mg-0.50Si	Al-2.07Fe -0.72Mg-0.45Si	0.9
0.6Mg-0.5Si	Al-1.8Fe -0.6Mg-0.5Si	Al-2.45Fe -0.79Mg-0.38Si	1.2

the Vickers hardness tester with a load of 200 gf and holding time of 10 s. The reported hardness values were based on the average of at least 5 measurements. Tensile tests were performed at ambient temperature using an mts landmark379 test system. The specimen had a gauge length of 45 mm and a gauge diameter of 10 mm. The testing was carried out with a tensile rate of 1 mm/min and a strain rate of  $3.7\times10^{-4}~\rm s^{-1}$ . At least 3 samples were performed to obtain the average yield strength (YS), ultimate tensile strength (UTS) and elongation of each alloy.

The electrical conductivity of alloys measured using PZ 60A eddy current conductivity meter operating at 60 kHz. The alloy surface was polished with 1200# and 2000# SiC sandpaper to remove the oxide layer and ensure the sample was sufficiently smooth. Each alloy was randomly tested at least 15 points to acquire precise conductivity values.

The thermodynamic calculations of the Al-Fe-Mg-Si system were performed using the Pandat software package with the PanAl thermodynamic database developed by CompuTherm LLC.

### 3 Results and discussion

### 3.1 The performance improvement and microstructure evolution of as-cast alloys

To clarify the effects of Mg and Si on the mechanical

properties of the Al-1.8Fe alloy, six samples were prepared in this work. These include 0Mg-0Si alloy (Al-1.8Fe), 0.45Mg-0Si alloy with only Mg added (Al-1.8Fe-0.45Mg), and 0.3Mg-0.5Si~0.6Mg-0.5Si alloys with different Mg/Si ratios (Al-1.8Fe-xMg-ySi). Stress-strain tests were carried out on the six as-cast alloys, and the results are shown in Figure 1(a). After adding 0.45 wt.% Mg, the yield strength (YS) and the ultimate tensile strength (UTS) of the Al-1.8Fe alloy both increased significantly, but the elongation (EL) slightly decreased. After the combined addition of Mg and Si, the mechanical properties of the alloy further increased. Compared with 0.45Mg-0Si alloy with only Mg added, the elongation did not decrease significantly. When the addition amount of Mg and Si exceeded ~1 wt.%, the UTS of the as-cast alloy reached a peak. Continuing to increase the addition amount of Mg and Si, the tensile strength of the as-cast Al-1.8Fe alloy remained at the same level. The test results of the mechanical properties of the alloy are shown in Figure 1 (b). Although the YS and UTS of the 0Mg-0Si alloy without Mg and Si are only 45.0±2.1 MPa and 110.2±0.1 MPa, the elongation reaches 34.0±3.7%. For the 0.45Mg-0Si alloy containing 0.45 wt.% of Mg, the YS increases to 52.0±3.1 MPa and the UTS increases to 142.3±4.2 MPa, but the elongation decreases to 25.7±0.6 %. The decrease in elongation may be caused by the addition of Mg changing the original phase composition in Al-1.8Fe. Noting that among the as-cast alloys with combined addition of Mg and Si, the 0.45Mg-0.5Si alloy with a Mg/Si ratio of 0.9 exhibits the best comprehensive mechanical properties. Its YS and UTS are 63.4±3.7 MPa and 184.8±2.4 MPa respectively, which are increased by 40.9 % and 67.7 % compared with the 0Mg-0Si alloy, and the elongation slightly decreases to 25.4±1.0 %.

The YS-EC distribution diagram of cast aluminum alloy is shown in Figure 1 (c). In cast conductive Al alloys, compared with Al-0.5Fe-X alloy<sup>[37]</sup>, Al-Mg alloy<sup>[38]</sup> and pure Al, the addition of Mg and Si brings a yield strength advantage in as-cast Al-1.8Fe alloy. The mechanical properties of Al-1.8Fe-xMg-ySi alloy reach the level of refined Al-Ni-Fe alloy. However, the decrease in electrical conductivity makes the alloy lose its performance advantage. After T6 heat treatment, both the electrical conductivity and yield strength of the alloy have significantly increased. This phenomenon will be analyzed in the subsequent.

To better reflect the influence of Mg and Si addition on the strength-ductility relationship of the Al-1.8Fe alloy and screen out the alloy composition with the best comprehensive performance, the strength-ductility product of six alloys was calculated and the electrical conductivity was tested. The results distribution of the strength-ductility product and electrical conductivity is shown in Figure 1(d). Due to the lowest content of solid solution elements in the matrix, the Al-1.8Fe alloy exhibits the best electrical conductivity performance, reaching 55±0.3 %IACS. With the introduction of Mg

and Si elements, the electrical conductivity of the alloy decreases sharply and remains at around 44 %IACS with the increase of Mg and Si. 0.45Mg-0.7Si, 0.45Mg-0.5Si, and 0.6Mg-0.5Si alloys are at the same electrical conductivity level. The strength-ductility products of alloys 0.45Mg-0.7Si, 0.45Mg-0.5Si, and 0.6Mg-0.5Si in the as-cast state all exceed 4 GPa%, reaching 4.4 GPa%, 4.7 GPa%, and 4.1 GPa% respectively.

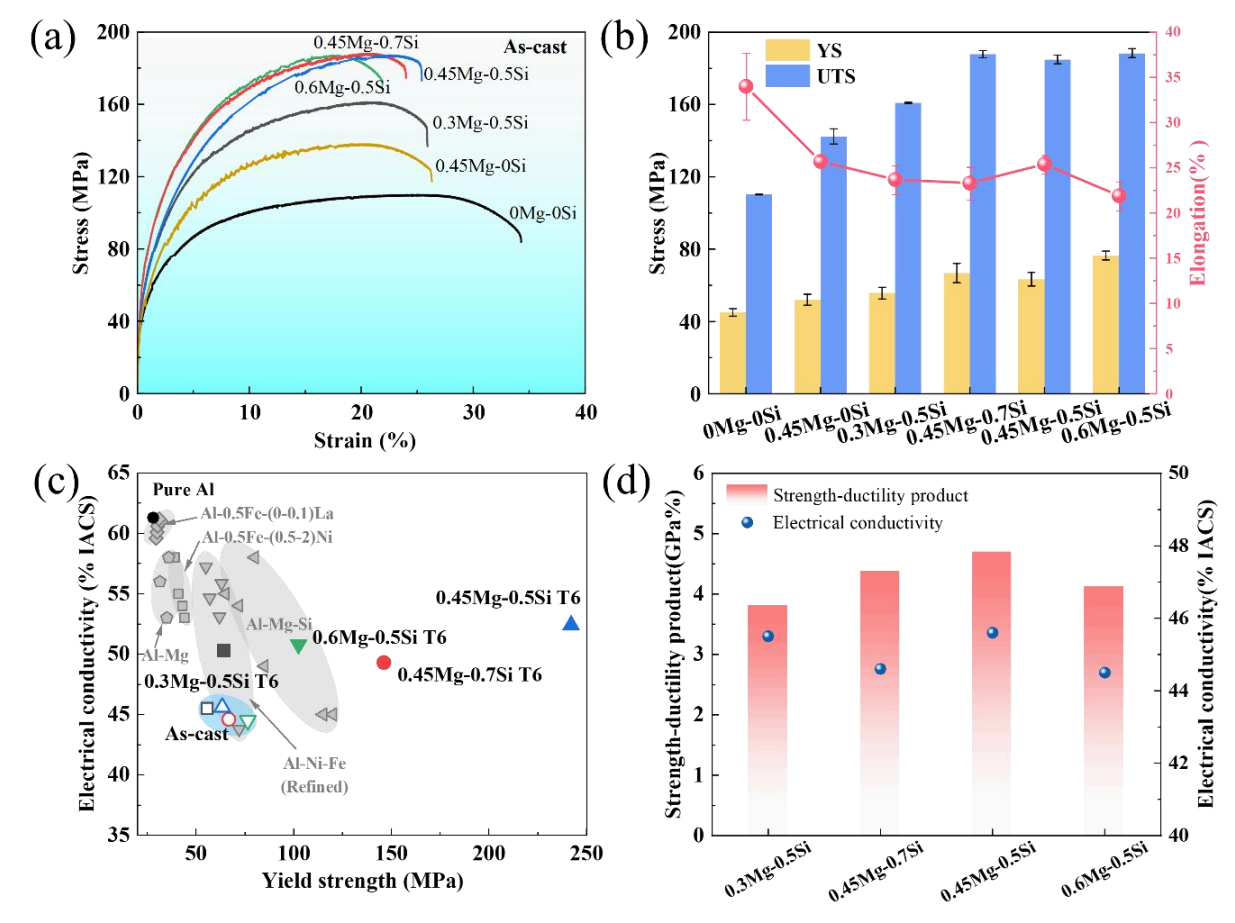


Figure 1 (a) The stress-strain curves of the as-cast Al-1.8Fe-xMg-ySi alloy, (b) mechanical properties of the Al-1.8Fe-xMg-ySi alloy, (c) the distribution of YS-EC for casting Al alloys, (d) the distribution of the strength-ductility products and EC in Al-1.8Fe-xMg-ySi alloy

To investigate the strengthening mechanisms of Mg and Si in as-cast Al-1.8Fe alloys, the microstructures of six samples were characterized by SEM-BSE, and the results are shown in Figure 2. The phase compositions of the alloys were analyzed by SEM-EDS, and the results are shown in Figure S1. Figure 2(a) and Figure 2(a1) show the morphology of the second phase of the Al-1.8Fe alloy. Due to the low solid solubility of Fe in the Al matrix, the Al - 1.8Fe alloy without the addition of Mg and Si forms a large number of fibrous rod-like Al-Fe binary intermetallic compounds, which are distributed in a dense network. Due to solute segregation, a small amount of granular second-phase is formed at the grain boundaries. Based on the results of SEM-EDS, the phase

in the alloy is determined to be the Al<sub>13</sub>Fe<sub>4</sub> phase. This eutectic structure with a network distribution does not disrupt the continuity of the matrix and can produce more uniform plastic deformation under stress. Therefore, the 0Mg-0Si alloy has the highest elongation, reached 34.0±3.7 %. The addition of Mg changed the morphology of the second phase, as shown in Figure 2(b) and Figure 2(b1). Different from 0Mg-0Si alloy, the second phase changed from dense fibrous rod-like to coarse lath shapes. Although the phase was still the Al<sub>13</sub>Fe<sub>4</sub>, strong stress concentration occurred at both ends of the lath-shaped second phase. It was prone to becoming a crack source during the deformation process. Therefore, the elongation of 0.45Mg-0Si alloy decreased significantly. At the same

time, the solid solution of Mg increased the lattice distortion in the Al matrix, leading to an increase in the strength of the alloy. The combined addition of Mg and Si in the Al-1.8Fe alloy resulted in new phases. As can be seen from Figure 2(c) and Figure 2(c1), in addition to the reticular eutectic structure in 0.3Mg-0.5Si alloy, lath-shaped AlFeSi phase and skeletal AlFeMgSi phase were also formed. The introduced new phases disrupted the continuity of the eutectic structure. When the total content of Mg and Si in the Al-1.8Fe alloy reaches about 1wt.%, a dense reticular structure is formed in the alloy,

as shown in Figure 2 (g-i) and Figure 2 (g1-i1). The three alloys 0.45Mg-0.7Si, 0.45Mg-0.5Si, and 0.6Mg-0.5Si have similar microstructures. In addition to the eutectic structure, the blocky phase is also formed. This phase is identified as the AlFeMgSi phase through SEM-EDS analysis. Due to the similar phase and microstructure, the 0.45Mg-0.7Si, 0.45Mg-0.5Si, and 0.6Mg-0.5Si alloys have similar mechanical properties, but there are slight differences in elongation. This may be caused by the different Mg/Si ratios resulting in different contents of the blocky phase.

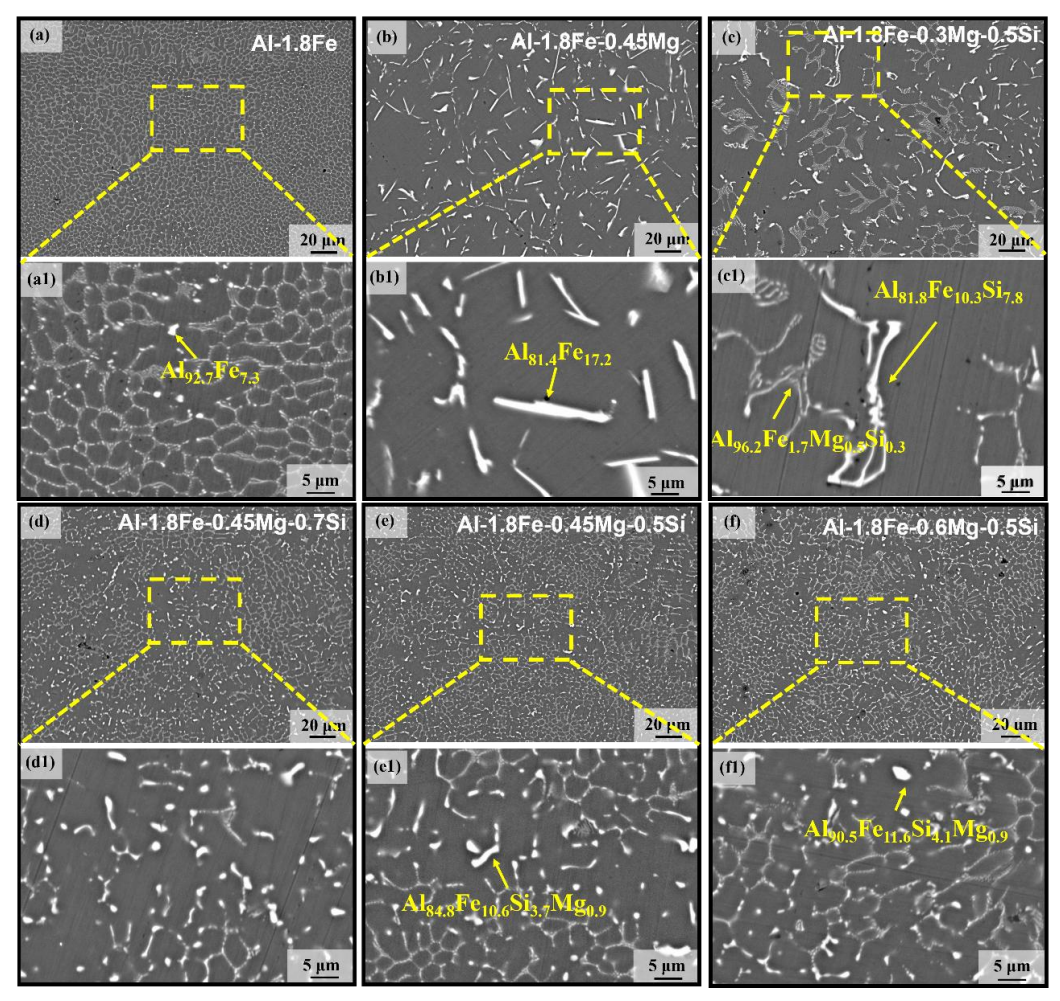


Figure 2 The SEM images of as-cast Al-1.8Fe-xMg-ySi alloy (a,a1) 0Mg-0Si, (b,b1) 0.45Mg-0Si, (c,c1) 0.3Mg-0.5Si, (d,d1) 0.45Mg-0.7Si, (e,e1) 0.45Mg-0.5Si, (f,f1) 0.6Mg-0.5Si

Further analyze the phases in the alloy through XRD. To facilitate the analysis of the second-phase composition, the spectral peaks were magnified, and the results are shown in Figure 3. The characteristic peak positions and peak intensities of the phases in these alloys are different, indicating that the phases and their contents in the Al-1.8Fe alloy have changed with the addition of Mg and Si and the change of their contents. When Al-1.8Fe alloy or only 0.45 wt.% Mg is added, only the characteristic peak of the Al<sub>13</sub>Fe<sub>4</sub> phase appears in the alloy. Mg is mainly dissolved in the Al matrix and provides solid

solution strengthening. When Mg and Si are added simultaneously, the phase composition changes, and the characteristic peaks of the  $\beta$ -AlSiFe phase and the  $\alpha$ -AlFeMgSi phase appear. As the Mg/Si ratio increases, the  $\beta$ -AlSiFe phase in the alloy gradually decreases, and the  $\alpha$ -AlFeMgSi phase gradually increases. When the Mg/Si ratio is greater than 1, the  $\beta$ -AlSiFe phase basically disappears, and the diffraction peak of the  $\alpha$ -AlFeMgSi phase is enhanced, indicating that the content of the  $\alpha$ -AlFeMgSi phase increases.

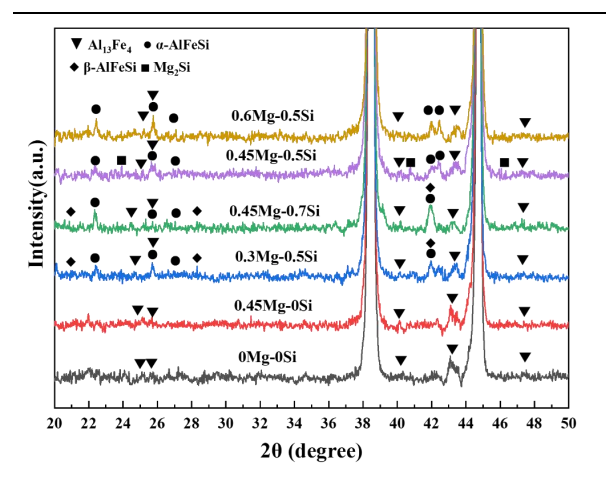


Figure 3 The XRD patterns of as-cast Al-1.8Fe-xMg-ySi alloys

The introduction of Mg and Si changes the properties of the cast Al-1.8Fe alloy in three aspects. Firstly, the solid solution of Mg and Si enhances the mechanical properties of the alloy. However, the atoms dissolved in the matrix increase electron scattering, resulting in a significant decrease in EC. Secondly, the combined addition of Mg and Si changes the types and contents of the second phase. The increase in the second phase is the main reason for the improvement of the mechanical properties. Thirdly, the Mg/Si ratio affects the microstructure of the alloy. As the Mg/Si ratio increases, the microstructure is refined. But more massive  $\alpha$ -AlFeMgSi phases are formed and leading to a decrease in the elongation.

### 3.2 The evolution of microstructure and properties during the heat treatment

Heat treatment is an important method to improve the mechanical properties of alloys<sup>[39-42]</sup>. At the same time, the nano-precipitation can reduce the solid solubility of elements in the matrix to a certain extent and decrease the electron scattering in the Al matrix<sup>[13]</sup>. Due to the addition of Mg and Si, the EC of the Al-1.8Fe alloy decreased from the initial 55.0±0.3 %IACS to 45.6±0.4 %IACS (0.45Mg-0.5Si alloy, Al-1.8Fe-0.45Mg-0.5Si). Although the mechanical properties are improved due to the increase of the second phase, the mechanical properties and EC still do not meet the requirements. Therefore, it is necessary to study the heat treatment properties of the Al-1.8Fe-*x*Mg-*y*Si alloy.

The T6 heat treatment was selected in this research. First, the samples were subjected to solution treatment at 520 °C for 4 h, then water-cooled to room temperature, and then aged at 180 °C. The hardness and EC during the solution treatment and aging process were tested. The

evolution of hardness and electrical conductivity of the six alloys during the T6 heat treatment is shown in Figure 4. The hardness of the 0Mg-0Si alloy without the addition of Mg and Si does not change with aging, indicating that the Al-1.8Fe alloy does not have the aging strengthening effect. The solid solution of Mg was increased in 0.45Mg-0Si alloy, but there was no improvement in performance during aging. Obviously, the introduction of Mg did not result in the formation of precipitation. It is worth noting that the EC of both 0Mg-0Si alloy and 0.45Mg-0Si alloy increased in the initial 1-4 hours of the aging process. This is attributed to the reduction of lattice defects, such as dislocations and vacancies, which reduced electron scattering and thus increased the EC.

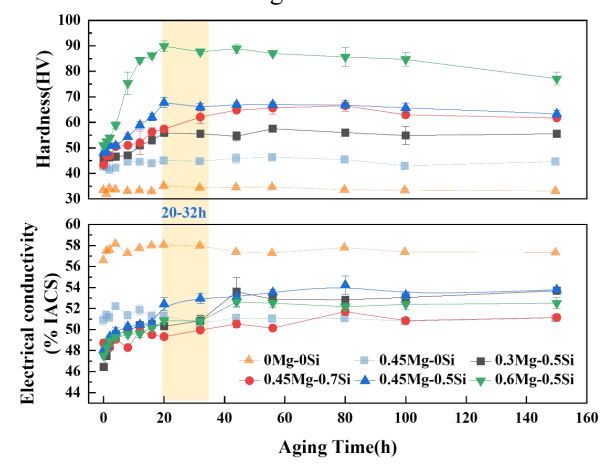


Figure 4 Age-hardening curves of Al-1.8Fe-xMg-ySi alloys

As a structural component in the precipitates of the Al-Mg-Si system, Si plays a crucial role in the nucleation and growth of precipitates<sup>[43-45]</sup>. After the composite addition of Mg and Si, the alloy exhibits obvious age-hardening effects within 0-20 h. The hardness of 0.3Mg-0.5Si alloy (Al-1.8Fe-0.3Mg-0.5Si) increased from 45.6 HV in the solution-treated state to 55.8 HV in the peak-aged state. The hardness of 0.45Mg-0.7Si alloy (Al-1.8Fe-0.45Mg-0.7Si) increased from 43.4 HV in the solution-treated state to 62.0 HV in the peak-aged state. hardness 0.45Mg-0.5Si of alloy (Al-1.8Fe-0.45Mg-0.5Si) increased from 48.2 HV in the solution-treated state to 67.8 HV in the peak-aged state. hardness 0.6Mg-0.5Si (Al-1.8Fe-0.6Mg-0.5Si) increased from 51.0 HV in the solution-treated state to 89.9 HV in the peak-aged state. With the extension of aging, the hardness of all alloys decreased to some extent and then tended to be stable. With the increase of strength, the EC of the four alloys showed a trend of gradually increasing and then stabilizing, reaching 53.9 %IACS, 50.9 %IACS, 53.8 %IACS and 52.5 %IACS, respectively. Unlike the trend of hardness change, the stabilization of EC shows a

certain hysteresis during the aging process. This is because after entering the over-aging stage, the  $\beta''$  phase transforms into the  $\beta$  phase, and the semi-coherent interface between  $\beta''$  and  $\alpha$ -Al is transformed into a

coherent interface between  $\beta$  and  $\alpha$ -Al<sup>[4]</sup>. As a result, the lattice distortion decreases and electron scattering is reduced.

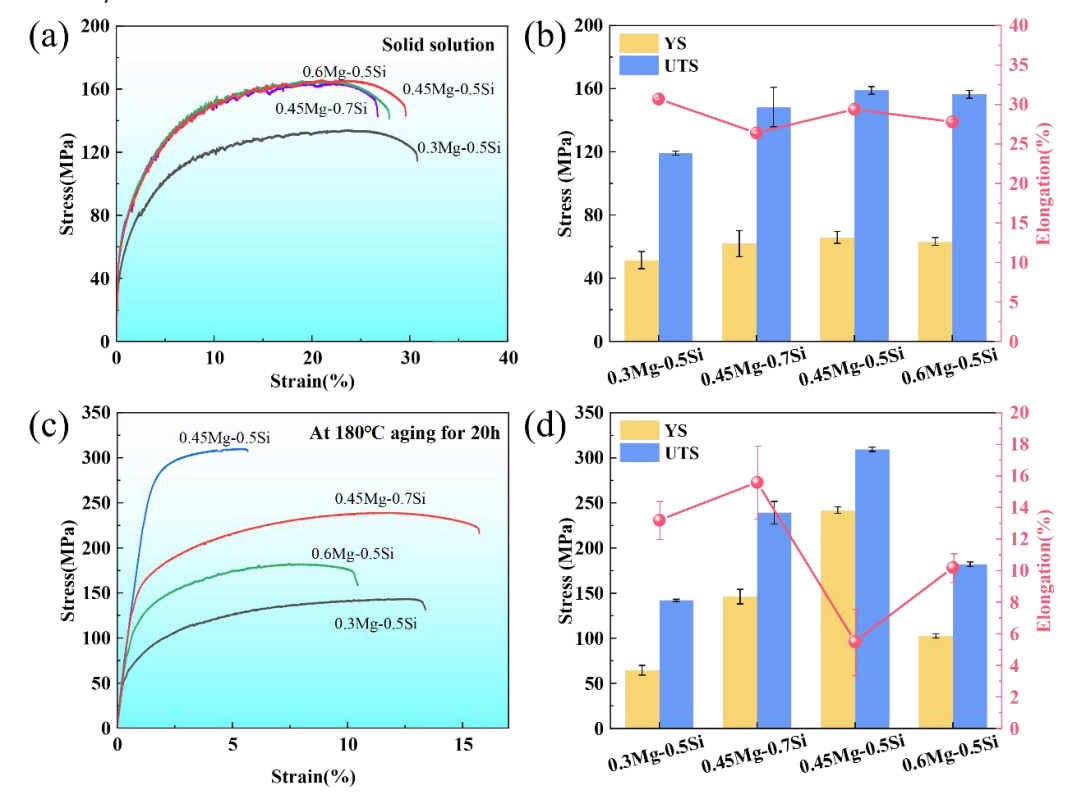


Figure 5 The stress-strain curves and mechanical properties of the Al-1.8Fe-xMg-ySi alloy under different heat treatment states (a-b) solution, (c-d) peak-aged

From the performance of hardness and EC, there is no positive correlation between the age-hardening effect of the alloy and the total amount of Mg and Si added. The age-hardening effect of the alloy can be improved by adjusting the Mg/Si ratio. The age-hardening effects of 0.45Mg-0.5Si alloy and 0.6Mg-0.5Si alloy are better than that of 0.45Mg-0.7Si alloy. That is, when the Mg/Si ratio is between 0.9 and 1.2, the Al-1.8Fe-xMg-ySi alloy has the optimal age-hardening effect.

The mechanical properties of the solution-treated 0.3Mg-0.5Si to 0.6Mg-0.5Si alloys are shown in Figure 5 (a-b). The YTS of the solution-treated alloys is decreased by ~40 MPa compared to that of the as-cast state. The mechanical properties of 0.45Mg-0.7Si to 0.6Mg-0.5Si alloys still remain at the same level. The difference is that due to the solution treatment causing partial dissolution of the second phase, the elongation of the alloy is increased.

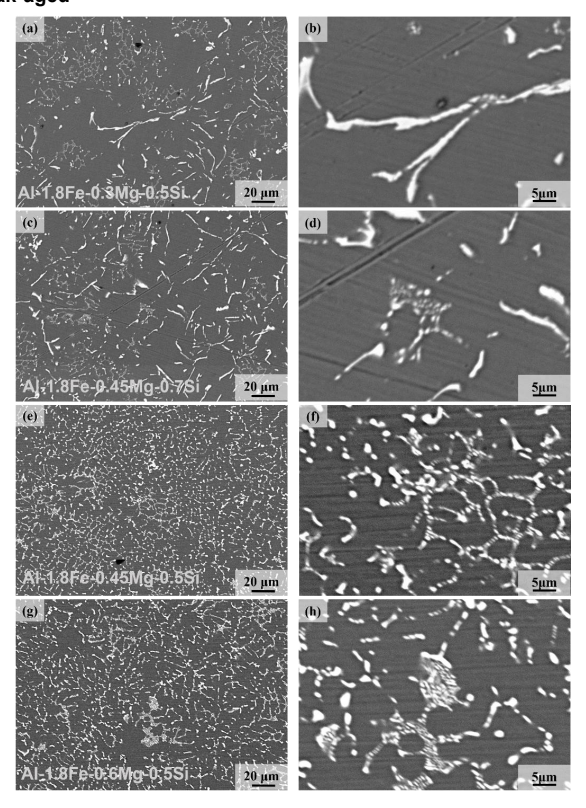


Figure 6 SEM images of solution Al-1.8Fe-xMg-ySi alloy (a-b) 0.3Mg-0.5Si, (c-d) 0.45Mg-0.7Si, (e-f) 0.45Mg-0.5Si, (g-h) 0.6Mg-0.5Si

Different Mg/Si ratios have a significant impact on the age-hardening effect of the alloy. The mechanical properties of the aged alloy are shown in Figure 5 (c-d). Different from the hardness, after 20 h of aging treatment, 0.45Mg-0.5Si alloy exhibits the best mechanical properties. The UTS and YS reach 309.5±5.6 MPa and 242.1±7.2 MPa, respectively, but the elongation decreases to 5.5±2.1 % after T6 heat treatment. 0.3Mg-0.5Si, 0.45Mg-0.7Si, and 0.6Mg-0.5Si alloys all exhibited different aging strengthening effects. Under the same time, the UTS increased by 22.9 MPa, 91.0 MPa, and 25.7 MPa, respectively, and the elongation decreased by 17.5%, 10.8%, and 17.6% respectively. When the Mg/Si ratio was 0.9, the Al-1.8Fe-0.45Mg-0.5Si alloy had the best aging strengthening in mechanical properties. When the Mg/Si ratio was 1.2, the Al-1.8Fe-0.6Mg-0.5Si alloy had the best hardness during aging.

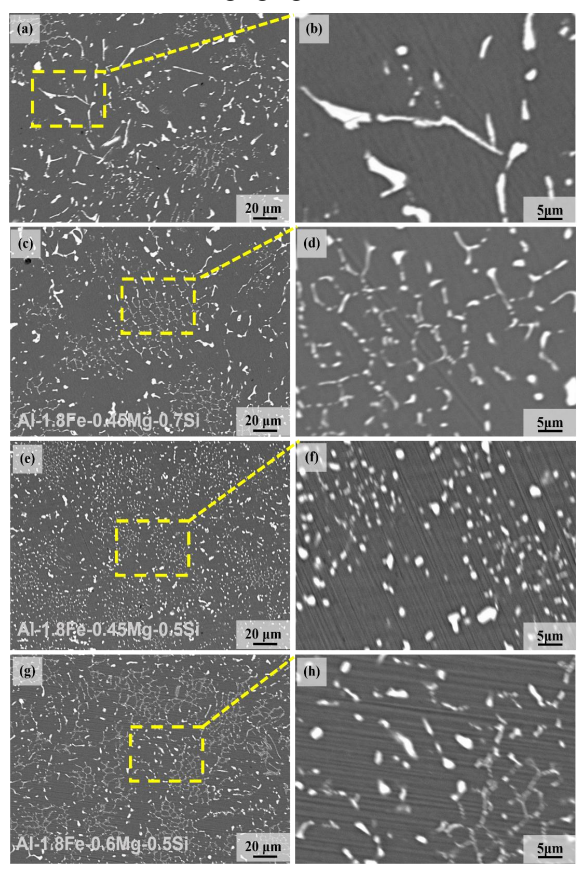


Figure 7 SEM images of peak-aged Al-1.8Fe-xMg-ySi alloy (a-b) 0.3Mg-0.5Si, (c-d) 0.45Mg-0.7Si, (e-f) 0.45Mg-0.5Si, (g-h) 0.6Mg-0.5Si

To further explain the influence of heat treatment on the properties, the microstructure of the alloy during the heat treatment was characterized by SEM, and BSE images of the solution-treated and aged microstructures were obtained. The results are shown in Figures 6 and 7. Compared with the as-cast alloy, after solution treatment at 520 °C, the fibrous rod-like eutectic structure and

massive second phase underwent spheroidization and coarsening, while the morphology of the lath-like second phase did not change significantly. Compared with the solution-treated microstructure, the second phase of the alloy after 20 h of aging underwent further coarsening, and the continuity of the eutectic structure was disrupted. It is worth noting that the morphology of the second phase in 0.45Mg-0.5Si alloy completely transformed into dispersed spherical particles after aging treatment.

## 3.3 The effect of the Mg/Si ratio on the age-strengthening of the Al-1.8Fe-xMg-ySi alloy

To investigate the influence of the Mg/Si ratio on the alloy microstructure, image segmentation was carried out on the microstructures of the alloy in different states, and classification was made according to the size of the second phase. The results are shown in Figure S2-S4. The aspect ratio and area fraction of the second phase were extracted and statistically analyzed, and the result are shown in Figure 8. The microstructure characteristics of the as-cast alloy are shown in Figure 8(a). With the addition of Mg and Si, the area fraction first decreases significantly and then gradually increases. From the distribution of the aspect ratio of the phases, when the Mg/Si ratio is greater than 0.6, the microstructure in the Al-1.8Fe-Mg-Si alloy is significantly refined, and the phase area fraction increases from 7.9 % of 0.3Mg-0.5Si alloy to more than 10 %. Among them, the phase area fraction of 0.45Mg-0.5Si alloy reaches 11.3 %. Through the solidification path calculation (Figure 9(a)), it can be known that the solid solution of Mg slows down the diffusion in the melt, expanding the solidification range of the Al-1.8Fe alloy from 1 °C to 206 °C. As a result, larger lath-shaped Al<sub>13</sub>Fe<sub>4</sub> phases are obtained. The combined addition of Mg and Si changes the original solidification path, generating α-AlFeMgSi phase and  $\beta$ -AlFeSi phase after  $\alpha$ -Al, which rapidly consumes Fe atoms in the melt and shortens the solidification range of the alloy to 100 °C.

The microstructural characteristics of the solution-treated and aged states are shown in Figure 8 (b-c). Heat treatment did not significantly change the phase area fraction. However, solution treatment led to a decrease in the aspect ratio of the second phase, resulting in spheroidization and coarsening. the second phase undergoes further spheroidization and coarsening after aging. Attributed to the difference in plasticity between the coarsened brittle second phase and the Al matrix, the second phase is prone to generating microcracks during the deformation and further expanding to cause fracture, resulting in the deterioration of the elongation after heat

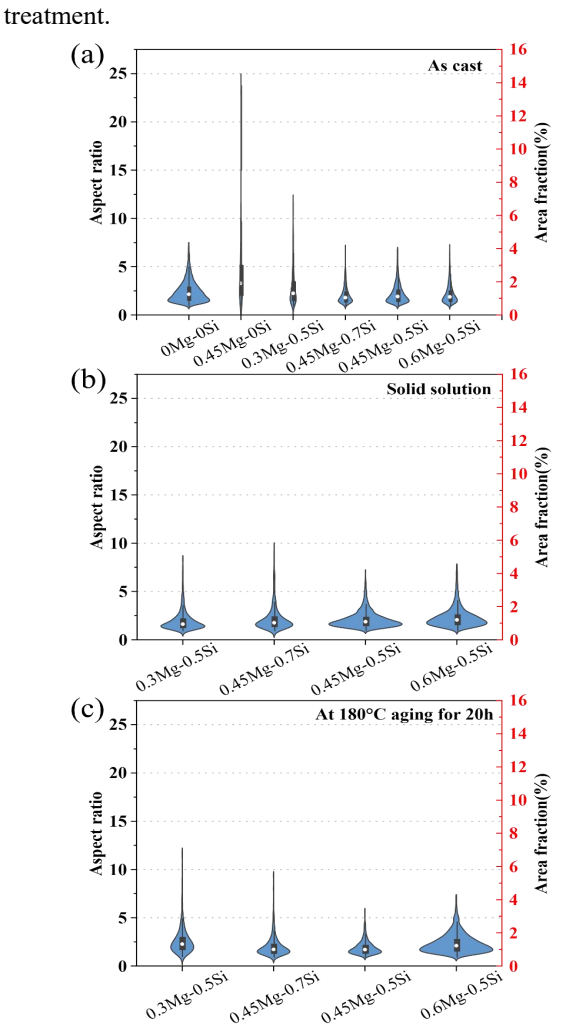


Figure 8The microstructure characteristics of the Al-1.8Fe-xMg-ySi alloy (a) as-cast, (b) solution, (c) peak-aged

From the results of hardness and mechanical properties, the age-hardening effect Al-1.8Fe-xMg-ySi alloy is affected by the total amount of Mg and Si and the Mg/Si ratio. When the Mg/Si ratio is 0.9, T6 heat treatment can significantly improve the mechanical properties of the alloy. When the Mg/Si ratio is 1.2, the contribution of heat treatment to hardness is significantly higher than that to strength, and the alloy hardness has the optimal age-hardening effect. To analyze the action mechanism of Mg and Si during the heat treatment, the distribution of elements in the as-cast, solution-treated and aged states was characterized by SEM-EDS, as shown in Figure S5-S7. The microstructure in the as-cast state exhibits obvious Si segregation. The segregation position of the Si coincides with the massive phase. After solution treatment, the segregation of the Si becomes more obvious, and Si enrichment occurs in the eutectic. There is no change after aging treatment. The Mg element shows a uniform distribution in the alloy. A small amount of segregated Mg<sub>2</sub>Si particles dissolve after solution treatment and enter the Al matrix. The solid

solubility of Mg and Si elements in  $\alpha$  - Al is shown in Figure 9(b), which varies significantly with temperature. In the matrix of 0.6Mg-0.5Si alloy, Mg maintains a high solid solubility at both 520 °C and 180 °C. Therefore, 0.6Mg-0.5Si alloy has the highest microhardness after heat treatment. During the aging process, the precipitates have a significant impact on the mechanical properties. By adjusting the Mg/Si ratio, the phase fraction of the Al-1.8Fe-Mg-Si alloy at 180°C can be changed, as shown in Figure 9(c). When the Mg/Si ratio in the alloy is between 0.9 and 1.2, the fraction of the  $\alpha$ -AlSiFe phase in the alloy reaches a stable level, and the content of the Mg<sub>2</sub>Si phase exceeds 0.7%. This provides high precipitation strengthening while ensuring the content of the second phase.

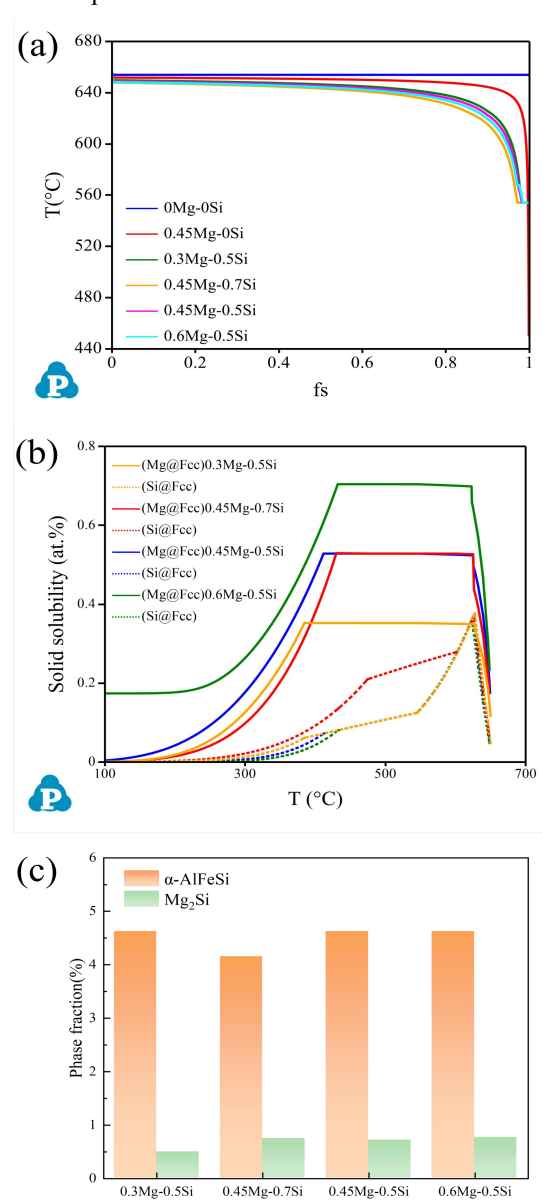


Figure 9 (a) The solidification paths of Al-1.8Fe-xMg-ySi alloy based on Scheil model, (b) The solid solubility of Mg and Si in  $\,\alpha$  -Al of Al-1.8Fe-xMg-ySi alloy, (c) The phase fraction calculated at 180  $\,^{\circ}\mathrm{C}$ 

EC and hardness distribution The of Al-1.8Fe-xMg-ySi alloy during aging are shown in Figure 10. Different Mg/Si ratios bring different degrees of improvement to the conductivity and hardness. When the Mg content is low and the Mg/Si ratio is also low, the aging treatment can significantly increase the EC, but the improvement of the alloy hardness is not obvious. When the Si content is high and the Mg/Si ratio is low, the aging treatment can increase both the conductivity and hardness of the alloy, but the improvement is not significant. By increasing the Mg/Si ratio in the alloy, when the Mg/Si ratio reaches 0.9-1.2, the aging treatment can significantly improve the strength and conductivity.

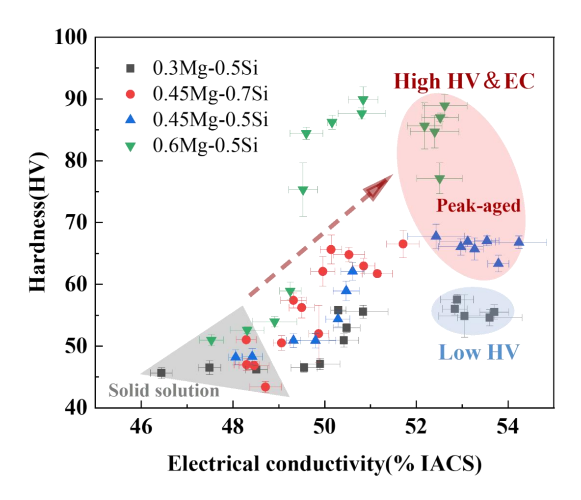


Figure 10 The electrical conductivity and hardness distribution of the Al-1.8Fe-xMg-ySi alloy during aging

### **4 Conclusions**

The effects of the addition of Mg and Si on the mechanical properties and electrical conductivity of the Al-1.8Fe alloy were investigated through SEM, XRD, and thermodynamic calculations, including as-cast and heat-treated states. By analyzing the properties and microstructures of alloys with different Mg/Si ratios during the heat-treatment, the corresponding relationship between the Mg/Si ratio and the age-hardening effect was established, and a casting Al-1.8Fe alloy with both high EC and high strength was obtained.

(1)The addition of Mg will increase the solidification range of the Al-1.8Fe alloy, resulting in the formation of coarse lath-like Al13Fe4 phase. The combined addition of Mg and Si can effectively refine the second phase, and new  $\beta$ -AlFeSi phase and  $\alpha$ -AlFeMgSi phase are formed, enhancing the second-phase strengthening effect of the alloy and improving its mechanical properties. However, the solid solution of elements will lead to a decrease in electrical conductivity.

(2)The combined addition of Mg and Si endows the Al-1.8Fe alloy with remarkable age-hardening. Solution

treatment causes the coarsening and spheroidization of the second phase, and age treatment further promotes this phenomenon. The continuity of the eutectic is disrupted, making the plastic deformation of the alloy non-uniform and leading to a rapid decrease in the elongation of the alloy.

(3)The Mg/Si ratio affects the age strengthening effect of the Al-1.8Fe-xMg-ySi alloy. When the Mg/Si ratio is 0.9, the alloy exhibits the optimal age strengthening effect. After T6 aging treatment, the Al-1.8Fe-0.45Mg-0.5Si alloy reaches a yield strength of 242.1 $\pm$ 7.2 MPa and a tensile strength of 309.5 $\pm$ 5.6 MPa at the peak aging state, and its electrical conductivity increases to 52.4 $\pm$ 0.6 %IACS.

### Acknowledgments

This work was financially supported by the National Natural Science Foundation of China (No. U2102212 and 52422407), the Chongqing Science and Technology Commission of China (CSTC2024YCJH-BGZXM0041) and the Major Scientific and Technological Innovation Project of CITIC Group (2022ZXKYA06100).

#### **Conflicts of interest**

The authors declare that they have no known competing financial interests or personal relationships that could have appeared to influence the work reported in this paper.

#### References

- [1] Zhan H, Zeng G, Wang Q, Wang C, Wang P, Wang Z, et al. Unified casting (UniCast) aluminum alloy—a sustainable and low-carbon materials solution for vehicle lightweighting. J. Mater. Sci. Technol. 2023;154:251-268.
- [2] Ramesh P and Lenin N C. High Power Density Electrical Machines for Electric Vehicles—Comprehensive Review Based on Material Technology. IEEE Trans. Magn. 2019;55:1-21.
- [3] Li Y, Hu A, Fu Y, Liu S, Shen W, Hu H and Nie X. Al Alloys and Casting Processes for Induction Motor Applications in Battery-Powered Electric Vehicles: A Review. Metals. 2022;12:216.
- [4] Khangholi S N, Javidani M, Maltais A and Chen X G. Review on recent progress in Al–Mg–Si 6xxx conductor alloys. J. Mater. Res. 2022;37:670-691.
- [5] Luo Z, Zhang X, Liu Z, Zhou H, Wang M and Xie G. Mechanical properties and interfacial characteristics of 6061 Al alloy plates fabricated by hot-roll bonding. Int. J. Miner. Metall. Mater. 2024;31:1890-1899.

- [6] Luo Q, Li X, Li Q, Yuan L, Peng L, Pan F and Ding W. Achieving grain refinement of α-Al and Si modification simultaneously by La–B–Sr addition in Al–10Si alloys. J. Mater. Sci. Technol. 2023;135:97-110.
- [7] Jeon J and Bae D. Effect of cooling rate on the thermal and electrical conductivities of an A356 sand cast alloy. J. Alloys Compd. 2019;808:151756.
- [8] Bakhtiyarov S I, Overfelt R A and Teodorescu S G. Electrical and thermal conductivity of A319 and A356 aluminum alloys. J. Mater. Sci. 2001;36:4643-4648.
- [9] Li Y, Jiang Y, Hu B and Li Q. Novel Al-Ti-Nb-B grain refiners with superior efficiency for Al-Si alloys. Scr. Mater. 2020;187:262-267.
- [10] Zhu L, Zhang Y, Luo Q, Peng L and Li Q. Effectively refining Al-10Si alloy via Al-Ti-Nb-B refiner with Nb2O5. J. Mater. Sci. Technol. 2024;176:204-210.
- [11] Yang Y, Nie J, Mao Q and Zhao Y. Improving the combination of electrical conductivity and tensile strength of Al 1070 by rotary swaging deformation. Results Phys. 2019;13:102236.
- [12] Pan L, Breton F and Fourmann J. Development of a new Al-Fe-Ni alloy for electric vehicle applications. Int. J. Metalcast. 2024;18:2841-2845.
- [13] Wang Y, Zhu L, Niu G and Mao J. Conductive Al alloys: the contradiction between strength and electrical conductivity. Adv. Eng. Mater. 2021;23:2001249.
- [14] Lunn K F and Apelian D. Thermal and Electrical Conductivity of Aluminum Alloys: fundamentals, structure-property relationships, and pathways to enhance conductivity. Mater. Sci. Eng., A. 2024;147766.
- [15] Dong Q, Wang R, Wang J and Nagaumi H. Influence of Mg/Si ratio on the mechanical strength and electrical conductivity of Al-Mg-Si alloys. Mater. Today Commun. 2025;42:111439.
- [16] Cui X, Ye H, Liu H, Li X, Man Q, Li H, et al. The improvement mechanism of good matching between electrical conductivity and mechanical properties for Al-4Si-0.8 Mg-0.6 Fe alloy. J. Alloys Compd. 2023;938:168275.
- [17] Wang H, Li Y, Zhang M, Gong W, Lai R and Li Y. Preheating-assisted solid-state friction stir repair of Al-Mg-Si alloy plate at different rotational speeds. Int. J. Miner. Metall. Mater. 2024;31:725-736.
- [18] Dong Q, Zhang Y, Wang J, Huang L and Nagaumi H. Enhanced strength-conductivity trade-off in Al-Mg-Si alloys with optimized Mg/Si ratio. J. Alloys Compd. 2024;970:172682.
- [19] Singh P, Ramacharyulu D A, Kumar N, Saxena K K and Eldin S M. Change in the structure and mechanical properties of Al-Mg-Si alloys caused by the addition of

- other elements: A comprehensive review. J. Mater. Res. Technol. 2023;27:1764-1796.
- [20] Li X, Scherf A, Heilmaier M and Stein F. The Al-rich part of the Fe-Al phase diagram. J. Phase Equilib. Diffus. 2016;37:162-173.
- [21] Jiang H, Li S, Zheng Q, Zhang L, He J, Song Y, et al. Effect of minor lanthanum on the microstructures, tensile and electrical properties of Al-Fe alloys. Mater. Des. 2020;195:108991.
- [22] Liu S F, Hu A, Hu H, Nie X and Kar N. Potential Al-Fe cast alloys for motor applications in electric vehicles: an overview. Key Eng. Mater. 2022;923:3-19.
- [23] Hou J, Li R, Wang Q, Yu H, Zhang Z, Chen Q, et al. Origin of abnormal strength-electrical conductivity relation for an Al–Fe alloy wire. Materialia. 2019;7:100403.
- [24] Jiang X, Zhang Y, Yi D, Wang H, Deng X and Wang B. Low-temperature creep behavior and microstructural evolution of 8030 aluminum cables. Mater. Charact. 2017;130:181-187.
- [25] Kim D, Kim J and Kobayashi E. Enhanced mechanical properties of Al-Si-Cu-Mg (-Fe) alloys by a deformation-semisolid extrusion process. Mater. Sci. Eng., A. 2021;825:141667.
- [26] Chen P, Fan X, Yang Q, Zhang Z, Jia Z and Liu Q. Creep behavior and microstructural evolution of 8030 aluminum alloys compressed at intermediate temperature. J. Mater. Res. Technol. 2021;12:1755-1761.
- [27] Gan L, Xiong Z, Cheng-bo L and Jun D. Design and preparation of Al-Fe-Ce ternary aluminum alloys with high thermal conductivity. Trans. Nonferrous Met. Soc. China. 2022;32:1781-1794.
- [28] Kong Y, Jia Z, Liu Z, Liu M, Roven H J and Liu Q. Effect of Zr and Er on the microstructure, mechanical and electrical properties of Al-0.4 Fe alloy. J. Alloys Compd. 2021;857:157611.
- [29] Shi Z, Gao K, Shi Y and Wang Y. Microstructure and mechanical properties of rare-earth-modified Al— 1Fe binary alloys. Mater. Sci. Eng., A. 2015;632:62-71.
- [30] Shin J-S, Ko S-H and Kim K-T. Development and characterization of low-silicon cast aluminum alloys for thermal dissipation. J. Alloys Compd. 2015;644:673-686.
- [31] Trink B, Weißensteiner I, Uggowitzer P J, Strobel K, Hofer-Roblyek A and Pogatscher S. Processing and microstructure-property relations of Al-Mg-Si-Fe crossover alloys. Acta Mater. 2023;257:119160.
- [32] Qin L, Tang P and Meng S. Effect of Ni addition on the microstructure, conductivities and mechanical properties of as-cast Al-Fe alloys. J. Alloys Compd. 2024;986:174160.
- [33] Zhang Y, Luo X, Zhu L, Chen Y, Luo Q, Xu J and Lu Q. Design of non-heat-treatable Al-Fe-Ni alloys with high

- electrical conductivity and high strength via CALPHAD approach. J. Alloys Compd. 2024;1009:176920.
- [34] Bian Z, Dai S, Wu L, Chen Z, Wang M, Chen D and Wang H. Thermal stability of Al–Fe–Ni alloy at high temperatures. J. Mater. Res. Technol. 2019;8:2538-2548.
- [35] Bian Z, Liu Y, Dai S, Chen Z, Wang M, Chen D and Wang H. Regulating microstructures and mechanical properties of Al–Fe–Ni alloys. Prog. Nat. Sci.: Mater. Int. 2020;30:54-62.
- [36] Kim J-M, Yun H-S, Shin J-S, Kim K-T and Ko S-H. Mold filling ability and hot cracking susceptibility of Al-Fe-Ni alloys for high conductivity applications. J. Teknol. (Sci. Eng.). 2015;75:2180-3700.
- [37] Kim J, Yun H, Shin J, Kim K and Ko e. Mold filling ability and hot cracking susceptibility of Al-Fe-Ni alloys for high conductivity applications. J. Teknol. 2015;75:71-77.
- [38] Jiang H, Li S, Zhang L, He J, Zheng Q, Song Y, et al. The influence of rare earth element lanthanum on the microstructures and properties of as-cast 8176 (Al-0.5Fe) aluminum alloy. J. Alloys Compd. 2021;859:157804.
- [39] Algendy A Y, Javidani M, Khangholi S N, Pan L and Chen X G. Enhanced Mechanical Strength and Electrical Conductivity of Al–Ni-Based Conductor Cast Alloys Containing Mg and Si. Adv. Eng. Mater. 2023;26:2301241.

- [40] Cui X L, Li X H, Ye H, Cui H W, Li H, Pan Y K, et al. Study on microstructure characterization, electrical conductivity and mechanical property improvement mechanisms of a novel Al-Si-Mg-Fe-Cu alloy. J. Alloys Compd. 2021;885:
- [41] Tang L, Wei P, Hu Z and Pang Q. Microstructure and mechanical properties stability of pre-hardening treatment in Al–Cu alloys for pre-hardening forming process. International Int. J. Miner. Metall. Mater. 2024;31:539-551.
- [42] Chen H, Sun J, Yang S, Zhang Y, Tang K, Zhang C, et al. Thermodynamics and kinetics of isothermal precipitation in magnesium alloys. MGE Advances. 2025;3:e86.
- [43] Xu X, Yang Z, Ye Y, Wang G and He X. Effects of various Mg/Si ratios on microstructure and performance property of Al-Mg-Si alloy cables. Mater. Charact. 2016;119:114-119.
- [44] Zhang B, Wu L, Wan B, Zhang J, Li Z and Gou H. Structural evolution, mechanical properties, and electronic structure of Al-Mg-Si compounds from first principles. J. Mater. Sci. 2015;50:6498-6509.
- [45] Marioara C D, Andersen S J, Hell C, Frafjord J, Friis J, Bjørge R, et al. Atomic structure of clusters and GP-zones in an Al-Mg-Si alloy. Acta Mater. 2024;269:119811.